ON PACKING LASER SCANNING MICROSCOPY IMAGES BY REVERSIBLE WATERMARKING: A CASE STUDY

Ioan-Catalin Dragoi [1] *Stefan G. Stanciu* [2] *Dinu Coltuc* [1] *Denis E. Tranca* [2]
Radu Hristu [2] *George A. Stanciu* [2]
[1] Electrical Engineering Department, Valahia University of Targoviste
[2] Center for Microscopy-Microanalysis and Information Processing, University Politehnica of Bucharest

ABSTRACT

Pairs of images of the same field-of-view collected by two complementary Laser Scanning Microscopy (LSM) work-modes are packed together by embedding one image of the pair into the other by reversible watermarking. One image remains visible and the other can be easily extracted at no extra transmission bandwidth cost. The packing keeps together the data without any risk of confusion. The use of reversible watermarking ensures, if necessary, the recovery of the host at zero distortion. Experimental results for Confocal Laser Scanning Microscopy (CLSM) and Transmission Laser Scanning Microscopy (TLSM) image pairs are provided.

Index Terms— LSM, CLSM, TLSM, reversible watermarking, prediction-error expansion

1. INTRODUCTION

The large variety of imaging systems and techniques currently available produce a large amount of data that must be stored, retrieved, transmitted and analyzed. In many cases, for the same object, sequences of images produced using various techniques and/or taken at different instances of time need to be collected. The general problem of dealing with large amount of images should be solved within the framework of specialized databases. On the other hand, particular solutions can also be developed to facilitate complementary image data management. In this context, we investigate the use of reversible watermarking to incorporate complementary 2D data into Laser Scanning Microscopy (LSM) images. We demonstrate this concept on pairs of Confocal Laser Scanning Microscopy (CLSM) and Transmission Laser Scanning Microscopy (TLSM) images of the same field-of-view and we investigate the embedding of the CLSM image into its TLSM counterpart. Thus, when a certain TLSM image is investigated, one can extract the embedded information and recover a copy of the associated CLSM image.

We remind that watermarking is the imperceptible hiding of information about a certain digital work within that work itself [1]. Besides the increase in security (copyright protection, fingerprinting, authentication), watermarking provides a transmission channel associated with some given data. The watermark becomes annotation data whose insertion in a host is meant to increase the value of the host.

While standard watermarking introduces permanent distortion, reversible watermarking not only extracts the embedded data, but also recovers the original host without any error. Nowadays image reversible watermarking algorithms and notably the prediction error expansion ones provide very good performances in terms of embedding bit-rate with respect to distortion. For instance, the embedding of up to 1 bit per pixel (bpp) is practically imperceptible to the human observer. An increase of the embedding bit-rate to about 1.5 bpp does not introduce annoying artifacts, but the watermarked image has a higher contrast than the original. Embedding bit-rates of 2-3 bpp can also be obtained, but at the cost of introducing noise and perceptible artifacts. On the other hand, since the embedding is reversible, the original host can be easily recovered at zero distortion. As far as we know, reversible watermarking has not yet been used in association with images collected by microscopy techniques although such digital image processing schemes could potentially provide multiple advantages with respect to microscopy data transfer, indexing and archiving.

The outline of the paper is as follows. The LSM images used in our experiment are presented in Section 2. A brief introduction of prediction-error expansion reversible watermarking is given in Section 3. Experimental results are presented in Section 4. Finally, the conclusions are drawn in Section 5.

2. LSM IMAGES

LSM Techniques represent essential tools for multiple fields of research. LSM variants such as Confocal Laser Scanning Microscopy or Multiphoton Laser Scanning Microscopy (MPLSM) provide the possibility to non-invasively acquire

The presented work was supported by the UEFISCDI PN-II-PT-PCCA-2011-3.2-1162 Research Grant (NANOLASCAN). The authors thank Dr. Mariana Costache (Carol Davila University of Medicine and Pharmacy, Bucharest, Romania) for providing the imaged tissue slides.

The second author thanks the financial support of the Sectoral Operational Programme Human Resources Development (SOP HRD), financed from the European Social Fund and the Romanian Government under the contract number POSDRU/159/1.5/S/13739.

978-0-9928626-3-3/15/$31.00 ©2015 IEEE

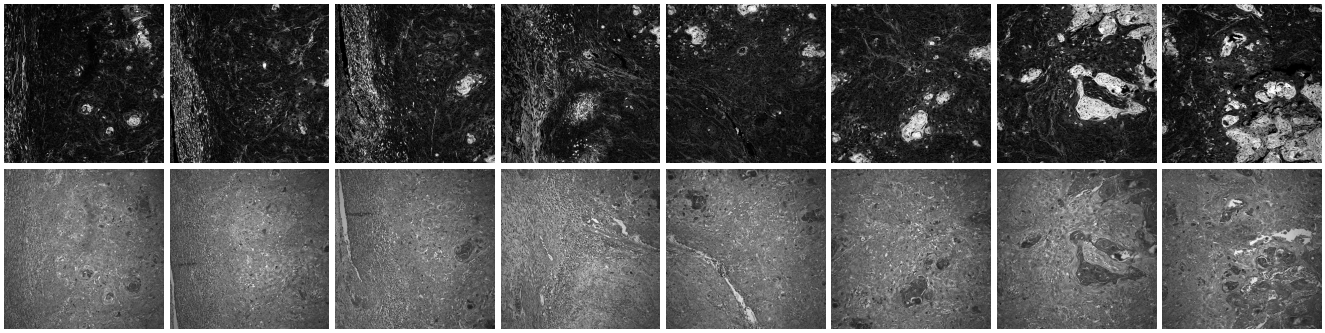

Fig. 1. Sequence of eight pairs of LSM images obtain through CLSM (first row) and TLSM (second row).

in-focus images from selected depths of both living and fixed specimens, which represents an enormous advantage for medicine and biology oriented imaging assays. In LSM the illumination light (a laser beam) is scanned onto the specimen point by point by a mirror on a galvano-motor-driven scanner and the light that is emitted from the specimen is likewise collected and de-scanned. The in-focus light reaches a photomultiplier tube (PMT), which detects light and converts photon hits into an analogue electron flow. Because of this specific image formation mechanism, the LSM images have different characteristics compared to natural images. These characteristics may lead to unpredictable results when image processing methods developed for natural images are used in their exact form for LSM images.

The LSM images that we used in this experiment were collected on a tissue slide stained with Hematoxylin-Eosin. The tissue fragment present on the slide was extracted from a skin tissue block affected by squamous-cell carcinoma. We have imaged multiple regions of this sample by using two LSM techniques: CLSM and TLSM. By CLSM we have imaged the fluorescent signal emitted by the investigated sample upon excitation with a laser beam of 488 nm wavelength, at a specific depth, while with TLSM we have imaged the transmitted excitation light (488 nm) through the corresponding specimen volume. An example of a sequence of eight image pairs collected with a 10x/0.42N.A. objective, providing a field of view of 1mm x 1mm is presented in Fig. 1.

3. PEE REVERSIBLE WATERMARKING

The prediction-error expansion (PEE) reversible watermarking scheme creates room for data embedding by increasing the prediction error [2]. The doubling of the prediction error causes the LSB (least significant bit) of the corresponding pixel to become zero and allows it to store a bit of data. Thus, the data and the auxiliary information are added to the expanded prediction error and embedded into the image. It should be noticed that the two times expansion of the prediction error provides an embedding bit-rate of less than 1 bpp. If higher embedding bit-rates are needed, a simple solution is the multilevel embedding, i.e., stages of embedding are chained until the required capacity is obtained. A better solution is the multibit embedding, where the prediction error is expanded n times in order to embed up to $\log_2 n$ bits of data per pixel.

Let us briefly present the basic principle of the PEE reversible watermarking [2]. Pixels are scanned (usually in raster-scan order) and, for each pixel $x_{i,j}$ the prediction error is computed as:

$$e_{i,j} = x_{i,j} - \hat{x}_{i,j} \tag{1}$$

where $\hat{x}_{i,j}$ is the predicted value of $x_{i,j}$.

A predefined threshold T is used to control the distortion introduced by the embedding. Only the pixels with $-T \leq e_{i,j} < T$ are used for embedding. The embedded pixel becomes:

$$x'_{i,j} = x_{i,j} + e_{i,j} + b_{i,j} \tag{2}$$

where $b_{i,j}$ is the data bit inserted in $x_{i,j}$.

The pixels with prediction errors that do not fulfill $-T \leq e_{i,j} < T$ are shifted in order to provide, at detection, a prediction error larger than the one of embedded pixels:

$$x'_{i,j} = \begin{cases} x_{i,j} + T & \text{if } e_{i,j} \geq T, \\ x_{i,j} - T + 1 & \text{if } e_{i,j} < -T. \end{cases} \tag{3}$$

The detection proceeds in reverse order, starting with the last embedded pixel. By computing the prediction error one distinguishes between the embedded and the shifted pixels. For the embedded pixels, the embedded bit is extracted as the LSB of the prediction error and furthermore, the original pixel is recovered. The shifted pixels are simply recovered by inverting equation (3).

Since the performance of the PEE reversible watermarking scheme depends on the quality of the predictor, a lot of effort has been devoted to improve the prediction. Very good results are obtained by using a simple noncausal predictor, the average on the rhombus composed of the four horizontal and vertical close neighbors [3]. Together with the threshold T, the variance of the prediction context is also used for embedding bit-rate control [3]. Since [3], many other PEE reversible watermarking schemes have been proposed [4]- [10], etc.

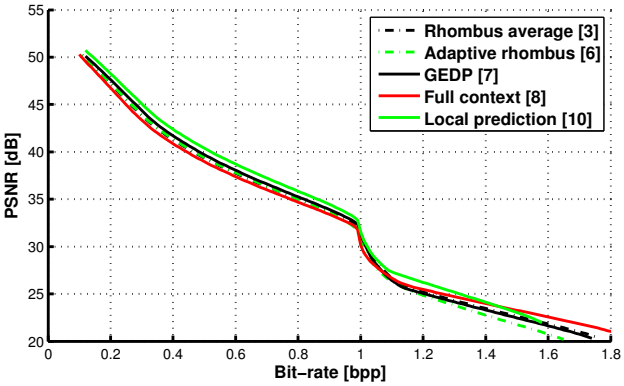

Fig. 2. Average results on the eight TLSM images for five reversible watermarking schemes.

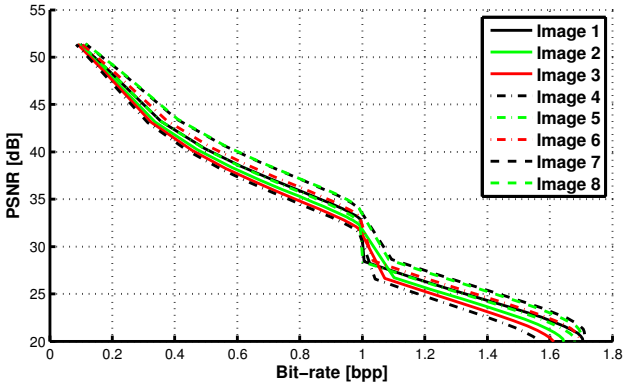

Fig. 3. Watermarking results on the TLSM images for the local prediction scheme.

We shall further consider the local prediction reversible watermarking scheme proposed in [10]. For each pixel, the optimal least square predictor is computed in a square block centered on the current pixel. The most interesting feature of the scheme is the fact that the predictor is recovered at detection without any additional information. The local prediction for rhombus context appears to provide outstanding results (see [10]). More precisely, it significantly outperforms on natural images the well-known scheme of [3] as well as many recently proposed schemes ([4]– [9], etc.). As will be shown in Section 4.1, similar results are obtained on the TLSM images.

4. EXPERIMENTAL RESULTS

We first investigate the capacity for data hiding provided by the sequence of TLSM images presented in Fig. 1 and then we examine the required data bit-rate for embedding the corresponding CLSM images. Examples of both embedded and recovered images are presented. Finally, the overall performance of the packing scheme is discussed.

4.1. Embedding bit-rate

Five well performing PEE based reversible watermarking schemes are considered for embedding in the TLSM image sequence: the rhombus average of [3], the adaptive rhombus of [6], the gradient-based edge direction prediction (GEDP) of [7], the full context predictor of [8] and the local prediction of [10] on the rhombus context. As can be seen from the results presented in Fig. 2, local prediction outperforms the other four watermarking schemes. On TLSM images the average difference in performance between local prediction and the other schemes is slightly smaller (around 0.5 dB) than on the natural images presented in [10]. Nevertheless, this gain in PSNR is consistent on all the tested TLSM images.

Next, let us discuss the embedding bit-rates offered by the local prediction reversible watermarking scheme. The bit-rate/PSNR graphs for the TLSM images from the sequence in Fig. 1 are presented in Fig. 3. Depending on the information content (complexity) of the host image, the maximum bit-rate offered by the watermarking scheme varies between 1.58 and 1.71 bpp. The maximum bit-rate can drop slightly bellow 1.4 bpp on some TLSM images. On the tested images, we found PSNRs larger than 30 dB for embedding bit-rates of about 1 bpp.

4.2. Compression bit-rates

Both TLSM and CLSM images are of 1024×1024 pixels, i.e., 1 MB size. The above results show that the reversible embedding is possible only after a considerable reduction of CLSM image sizes. A straightforward solution for trading between the size and quality of an image is provided by lossy image compression. We have considered the lossy compression provided by JPEG 2000. The results on the sequence of eight CLSM images are plotted in Fig. 4. The compressed CLSM image can be successfully embedded into its TLSM counterpart, if the embedding bit-rate provided by the TLSM image is equal or larger than the compression bit-rate of the CLSM image. In order to minimize the distortion of the host image, it is preferable to keep the difference between the two bit-rates as small as possible.

4.3. Embedding results

The results of Sections 4.1 and 4.2 show that there is enough room for embedding by reversible watermarking in the TLSM images good quality versions of the corresponding CLSM images. As proposed above, one should look for a compromise between the quality of the compressed image and of the embedded one.

Two scenarios should be taken into account: (i) the user is interested in the additional CLSM image data; (ii) the user is not interested in the embedded data. The first scenario supposes the extraction of the embedded data and the decompres-

Table 1. Average PSNR results for the sequences of compresed CLSM images and watermarked TLSM images.

Bit-rate [bpp]	Average PSNR [dB]							
	Sequence 1		Sequence 2		Sequence 3		Sequence 4	
	CLSM	TLSM	CLSM	TLSM	CLSM	TLSM	CLSM	TLSM
0.7	26.53	37.21	26.91	36.81	25.47	38.73	25.64	39.23
0.8	26.97	35.84	27.46	35.12	25.96	37.14	26.14	37.76
1	27.86	31.54	28.53	29.85	26.9	32.47	27.11	32.97
1.2	28.82	26,22	29.62	26.15	27.89	27.57	28.08	28.7
1.3	29.32	25.17	30.2	24.79	28.43	25.95	28.56	27.54

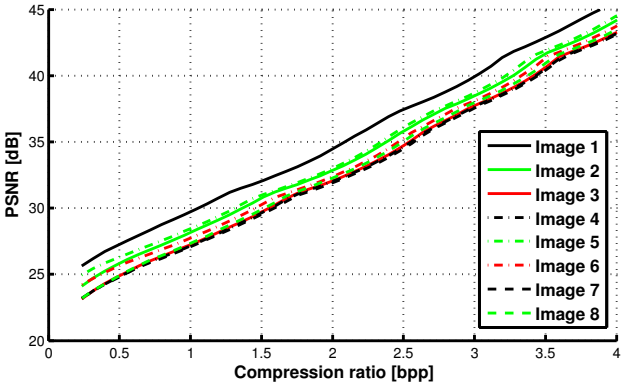

Fig. 4. Compression results on the eight CLSM images

sion of the CLSM images. As a byproduct of the detection and decoding procedure, one has the recovery of the host sequence at zero distortion. Since the quality of both sequences do count and since the host images can be exactly recovered, one could embed at higher bit-rates.

In the second scenario, only the host images are examined. If their quality is not good enough (because of watermarking distortions), one should decode the embedded data and recover the original. Obviously, the exact recovery is possible, but at the cost of decoding and extracting the data.

An example for embedding two low resolution versions of the second CLSM image of Fig. 1 (from left to right) is provided in Fig. 5. While the results are given for the entire image, in order to ensure good visibility only a quarter of the image is shown in Fig. 5. The original TLSM image is presented in Fig. 5.a. Two lossy compressed versions are shown in 5.b (0.783 bpp, 27.16 dB) and 5.c (1.478 bpp, 30.63 dB), respectively. While for image 5.b one can observe by zooming a mild loss of edge clarity, no artifacts are visible for image 5.c. Furthermore, the two compressed versions are embedded into the corresponding TLSM image (Fig. 5.d). No artifacts can be seen for the watermarked image in Fig. 5.e (0.783 bpp at 35.15 dB), while the one in Fig. 5.f (1.478 bpp at 23.2 dB) is slightly noisy. As said above, the original versions of Fig. 5.e and Fig. 5.f can be immediately restored. The visual quality of the embedded images is better than one can suppose by looking at the PSNR. This is due to the fact that PEE watermarking introduces less distortion in uniform areas than in nonuniform areas. Obviously, the human visual system is more sensitive to errors in uniform areas than in textured ones.

The presented results show that image pairs collected by complementary LSM techniques can be packed together using a watermarking inspired strategy. We have demonstrated this concept by inserting into TLSM images, their corresponding CLSM pairs collected on the same field of view. The quality of the two images is easily controlled by tunning the compression bit-rate. As shown above, no artifacts have been noticed. Similar results have been obtained in all our tests on sequences of LSM images of skin tissue affected by squamous-cell carcinoma. The average PSNRs for the sequence of Fig. 1 (sequence 1) and three other sequences for some key bit-rates are summarized in Table 4.3. The trade off between the quality of compressed CLSM image and the quality of its TLSM host is easily noticeable in this table. For a bit-rate of 1 bpp, a good quality for the TLSM image is maintained (an average PSNR above 31 dB for three of the four sequences), while obtaining an acceptable version of the CLSM image (27 dB). The bit-rate can be increased to improve the quality of the compressed image (28–30 dB) at a significant cost to the quality of the (easily recoverable) host image (24–27 dB).

5. CONCLUSIONS

The use of reversible watermarking for packing together LSM images of the same field-of-view collected by complementary LSM workmodes has been examined. The proposed approach was demonstrated for pairs of TLSM and CLSM images, providing together with the TLSM image the additional CLSM data without demanding extra transfer bandwidth or time. From our experiment it appears that the reversible watermarking provides enough room for hiding in the TLSM images good quality compressed CLSM images. The use of reversible watermarking ensures, if necessary, the recovery of the host images at zero distortion.

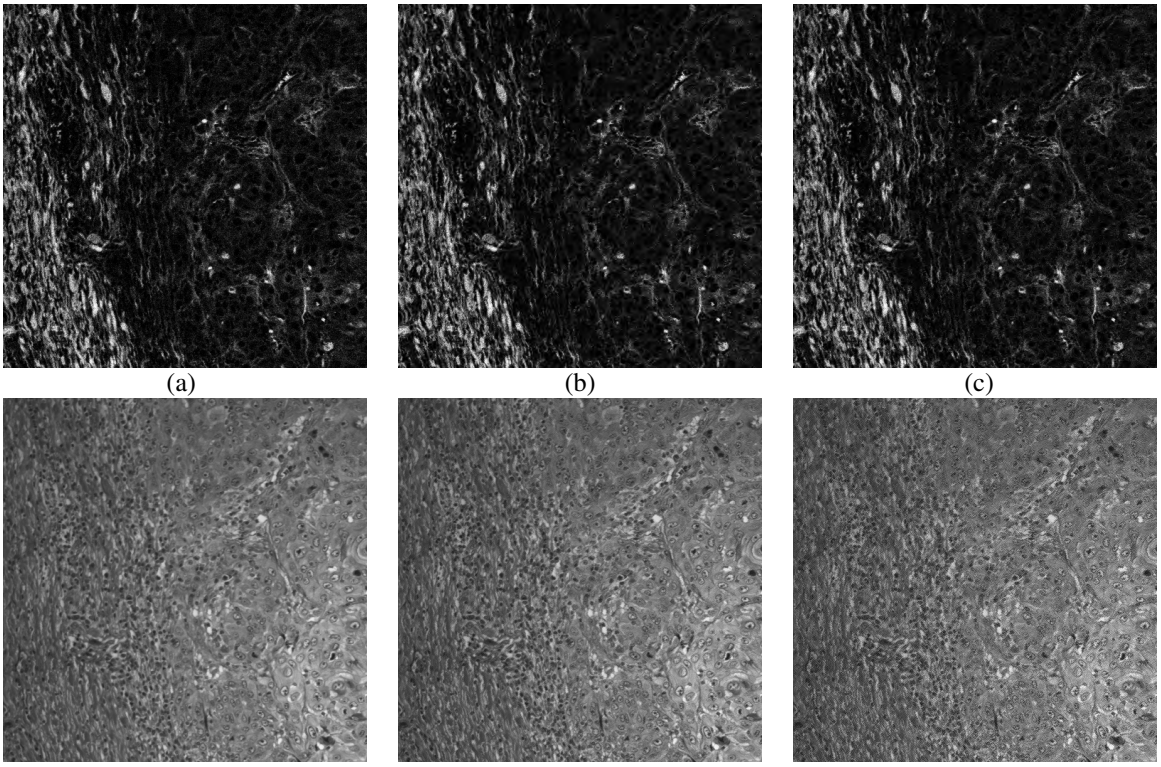

Fig. 5. First row - original CLSM image (a) and compressed versions at 0.783 bpp (b) and 1.478 bpp (c); Second row - original TSLM image and watermarked versions with 0.783 bpp (e) and 1.478 bpp (f).

REFERENCES

[1] I. J. Cox, M. L. Miller, J. A. Bloom, J. Fridrich and T. Kalker, *Digital Watermarking and Steganography*, Morgan Kaufmann Publishers, 2008.

[2] D. M. Thodi and J. J. Rodriguez, "Expansion Embedding Techniques for Reversible Watermarking", *IEEE Trans. Image Process.*, vol. 15, pp. 721–729, 2007.

[3] V. Sachnev, H. J. Kim, J. Nam, S. Suresh and Y. Q. Shi, "Reversible Watermarking Algorithm Using Sorting and Prediction", *IEEE Trans. Circuits Syst. Video Technol.*, vol. 19, pp. 989–999, 2009.

[4] D. Coltuc, "Improved Embedding for Prediction Based Reversible Watermarking", *IEEE Trans. Inf. Forensics Security*, vol. 6, no. 3, pp. 873–882, 2011.

[5] X. Li, B. Yang and T. Zeng, "Efficient Reversible Watermarking Based on Adaptive Prediction-Error Expansion and Pixel Selection", *IEEE Trans. on Image Process.*, vol. 20, no. 12, pp. 3524–3533, 2011.

[6] I.-C. Dragoi and D. Coltuc, Improved Rhombus Interpolation for Reversible Watermarking by Difference Expansion, *Proc. 20th European Conf. on Signal. Process., EUSIPCO2012*, pp. 1688–1692, 2012.

[7] W.-J. Yang, K.-L. Chung, H.-Y. M. Liao and W.-K. Yu, "Efficient reversible data hiding algorithm based on gradient-based edge direction prediction", *Journal of Systems and Software*, vol. 86, no. 2, pp. 567–580, 2013.

[8] X. Li, B. Li, B. Yang and T. Zeng, "General Framework to Histogram-Shifting-Based Reversible Data Hiding", *IEEE Trans. on Image Process.*, vol. 22, no. 6, pp. 2181–2191, 2013.

[9] W. Zhang, X. Hu, X. Li, and N. Yu, "Recursive Histogram Modification: Establishing Equivalency between Reversible Data Hiding and Lossless Data Compression", *IEEE Trans. on Image Process.*, vol. 22, no. 7, pp. 2775-2785, 2013.

[10] I.-C. Dragoi and D. Coltuc, "Local Prediction Based Difference Expansion Reversible Watermarking", *IEEE Trans. on Image Processing*, vol. 23, no. 4, pp. 1779–1790, 2014.